Comparison of interactive and automatic segmentation of stereoelectroencephalography electrodes on computed tomography post-operative images: preliminary results

Sahar Benadi, Irene Ollivier, Caroline Essert

▶ To cite this version:

Comparison of interactive and automatic segmentation of stereoelectroencephalography electrodes on computed tomography post-operative images: preliminary results

Sahar Benadi[1,2], Irene Ollivier[3], Caroline Essert[1] ✉

[1]*ICube, Université de Strasbourg, CNRS, Strasbourg, France*
[2]*Telecom Physique Strasbourg, Strasbourg, France*
[3]*Department of Neurosurgery, Strasbourg University Hospital, Strasbourg, France*
✉ *E-mail: essert@unistra.fr*

Stereoelectroencephalography is a surgical procedure used in the treatment of pharmacoresistant epilepsy. Multiple electrodes are inserted in the patient's brain in order to record the electrical activity and detect the epileptogenic zone at the source of the seizures. An accurate localisation of their contacts on post-operative images is a crucial step to interpret the recorded signals and achieve a successful resection afterwards. In this Letter, the authors propose interactive and automatic methods to help the surgeon with the segmentation of the electrodes and their contacts. Then, they present a preliminary comparison of the methods in terms of accuracy and processing time through experimental measurements performed by two users, and discuss these first results. The final purpose of this work is to assist the neurosurgeons and neurologists in the contacts localisation procedure, make it faster, more precise and less tedious.

1. Introduction: Pharmacoresistant epilepsy is a complicated illness that can sometimes be curable by resorting to a surgical intervention, after performing a stereoelectroencephalography (SEEG) to detect the seizure onset zone [1]. SEEG procedure consists of inserting electrodes in the patient's brain to record the electrical activity within the brain parts that are likely to be responsible for the seizures.

After this intervention, a post-operative computed tomography (CT) image is acquired to assess if the electrodes and their recording contacts are placed as planned. The localisation of electrodes contacts is a crucial step in the post-SEEG phase since the next surgical intervention aiming at destroying the epileptogenic zone by performing a radio-frequency thermocoagulation [2] or by excising that zone is based on its accurate localisation. However, the contacts localisation and identification is difficult and time-consuming, especially when the neurosurgeon has to process a large number of slices, and there is a high number of implanted electrodes. To help the surgeon with this task, a limited number of groups have recently started to investigate the automatic segmentation of SEEG [3, 4]. A comparison with their works is proposed in the discussion. Other studies have been proposed for deep brain stimulation [5] electrodes, with a lower number of contacts and electrodes involved in the process.

In this Letter, we present an automatic segmentation algorithm that we have developed. It takes post-operative CT images as an input (an example of these images is given in Fig. 1 below), then performs a succession of processing steps in order to detect the different electrodes and provide the surgeons with the location of the contact.

We have also implemented two versions of simple and intuitive interactive segmentation processes that require minimal interaction from the surgeon. The objective is two-fold: the results of these methods will be used as a reference for the proposed automatic segmentation to be validated and will be compared with assessing the interest of automatic methods. In the next sections, we will expose the principle of each of the interactive and automatic segmentations, preliminary results obtained in each case and a first comparison between the methods. Finally, we will conclude this Letter by briefly discussing the performance and the limitations of the proposed methods that can already be outlined with these first results.

Before presenting our approaches, we give below the definitions of a few concepts that will be used throughout this Letter (compare Fig. 1):

Electrode: metallic contacts and screw attached to the skull.
Entry point: the position where the electrode is inserted into the skull.
Target point: the position of the deepest contact of the electrode.
Trajectory length: distance between target and entry point.
Contact length: distance between the first and the last contacts of the electrode.

2. Materials and methods

2.1. Development platform: The development of the automatic and interactive algorithms has been carried out using 3D Slicer (version 4.9.0) which is an open-source software where the user can elaborate his own image processing module depending on his project purposes and integrate it into the software to visualise the results [6]. We implemented Python scripted modules to perform the interactive and automatic segmentations.

2.2. Interactive segmentation: For the neurosurgeon, the interactive segmentation consists of localising the contacts using clicks with the mouse. The first method allows the user to point at all the contacts centres one by one with the mouse on the CT images volume, as they appear relatively clearly as white dots on the image (see Fig. 2). A specific user interface has been developed within the interactive segmentation module. After a short setup, the user clicks the points and the module creates a small cylinder around each of them, calculates the trajectory and contact lengths. This method is tedious, but in the case of electrode bending the contacts is more precisely pointed. In the rest of this Letter, we will also refer to this method as the *one-by-one interactive* method.

The second interactive method is designed to require less interaction and reduce segmentation time. The neurosurgeon simply
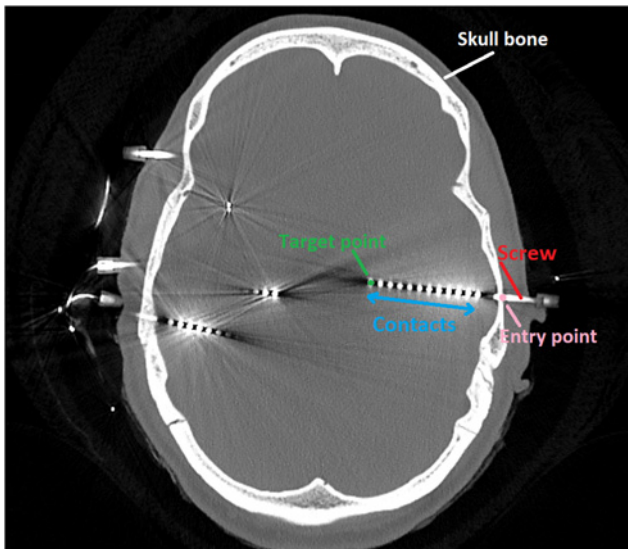
Fig. 1 *Example of a CT post-operative image in SEEG*
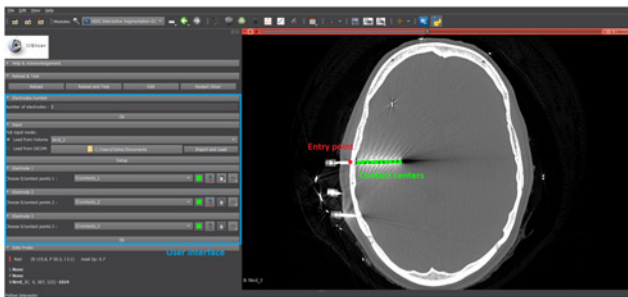
Fig. 2 *Interactive segmentation: entry point (red), contact centres (green) that are placed interactively by the surgeon through the created user interface (blue) in 3D Slicer*

has to click on the entry point of the electrode and its target point, and a cylinder is placed between them. This method is faster; however, it produces only straight electrode shapes. In the rest of this Letter, we will also refer to this method as the *fast interactive* method.

2.3. Automatic segmentation

2.3.1 Preprocessing of the CT post-operative images: Preprocessing the images is a crucial step before implementing the electrodes detection algorithm. Indeed, the presence of parts that have the same intensity level as that of the electrodes (essentially external wires) highly affects the good detection of the SEEG contacts. The preprocessing is carried out without any interaction from the user. First, thanks to the 3D Slicer module named *Foreground Masking*, a mask of the head with the implanted SEEG electrodes is created in order to isolate the foreground parts of the CT images (brain, electrodes and skull bone) from the background elements (wires). Then, the created mask is adjusted in a way that makes it cover exactly and only the foreground parts using the *Segment Editor* module. Finally, the mask is applied to the image so that the background voxels are set to zero using the *Mask Scalar Volume* module. The modules are called automatically within the algorithm, resulting in a completely automated pipeline. Fig. 3 shows illustrations of the preprocessing steps.

2.3.2 Automatic detection of the electrodes and contacts: Automatic detection of the electrodes is performed on the preprocessed images. First, we segment the images volume using the
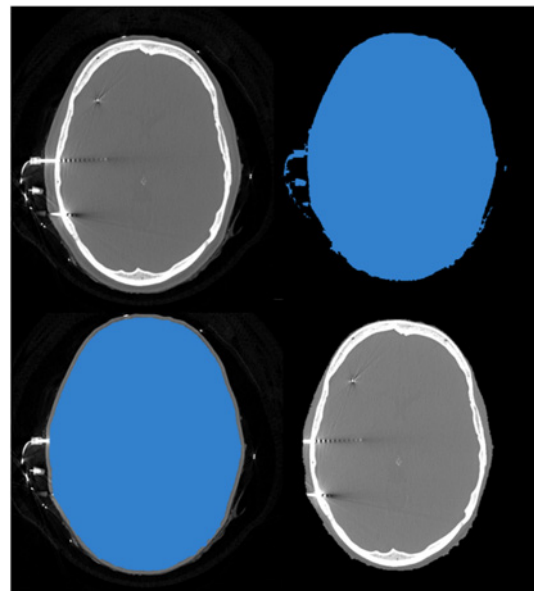

Fig. 3 *Preprocessing steps: original image (top-left), the creation of the foreground mask (top-right), adjustment of the mask (bottom-left) and mask application (bottom-right)*

SimpleITK *Binary Threshold Image Filter*, with the CT images maximum intensity chosen as the upper threshold, and 2600 as a lower threshold, based on CT images histograms. This large value was chosen as providing a good detection for the remaining bright elements other than electrodes (such as skull bone) to be eliminated. Then, the *Connected Component (CC) Image Filter* is applied to separate the CCs. The resulting CC is automatically labelled to facilitate their identification. Then, a process in three steps allows to identify and classify the electrodes and their respective contacts:

Step-1. Extraction of the electrodes screws.
Step-2. Computation of the electrodes major axes.
Step-3. Contacts classification.

The results of the different steps above are illustrated in Fig. 4. Among the labelled CC, electrode screws are separated from the contacts using size as a criterion (Fig. 4, step-1): small CC corresponds to contacts, while large CC corresponds to screws. Before selecting the CC corresponding to screws, we delete very large
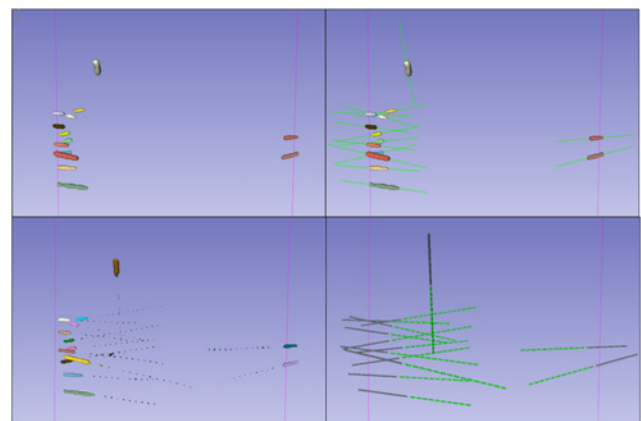

Fig. 4 *Automatic segmentation steps: step-1 (top-left) screw extraction, step-2 (top-right) PCA of screw models, step-3 (bottom-left) contacts classification and step-4 (bottom-right) electrode models' adjustment*

and very small components for the screws size computation to be more accurate. Then, we consider as a screw every CC bigger than one-third of the largest CC size among the remaining CC. We do thereafter a principal component analysis (PCA) on each screw to determine its major axis (Fig. 4, step-2). Each of the CC corresponding to a contact is then assigned to a screw by evaluating its proximity with the screw's axis (Fig. 4, step-3). We obtain sets of screw/contacts corresponding to full separate electrodes. Moreover, contacts assignment is performed in order from the nearest contact to the farthest one regarding the electrode's screw. This order is important for the electrode contacts to be easily identifiable. At that point, the contacts are grouped into sets corresponding to the electrodes. They can possibly follow a slightly bended trajectory in some cases.

However, contact classification might sometimes have inaccuracies due to the presence of artefacts on the CT images. This problem may happen when two electrodes are close to each other, as illustrated in Fig. 5.

A variant of this method is proposed to overcome this issue. It also allows to visualise the electrodes with a geometry that is closer to their actual specifications. For this, we add a fourth step:

Step-4: Adjustment of the electrodes axes and reconstruction of the electrodes with respect to their geometrical characteristics.

It consists of adjusting the electrodes axes by considering the line that links the last contact to the first one. Finally, a reconstruction of the geometry is performed, thanks to their characteristics given by the SEEG electrodes manufacturer. Small cylinders are placed and evenly spaced using the specifications of the electrode model. This allows correcting the errors due to the multiple segmentation processes and artefacts. The appropriate electrode model is determined by comparing the distance from the first to the last contact and the number of contacts with the specifications of the models.

However, in some cases, it may occur that not all of the contacts of an electrode are detected, hence the electrode reconstruction and recognition are not accurate. For example, the electrode shown in Fig. 6 is supposed to be a 15-contact electrode, but at Step-3 we obtain a set of screw/contacts containing only four contacts. Possible solutions to that problem are to use adaptive thresholding parameters, and/or to try to infer the electrode
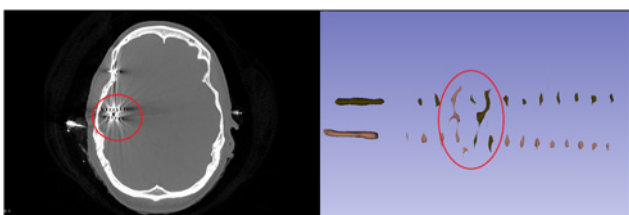

Fig. 5 *Influence of artefacts (within red circles) on the automatic classification of electrodes contacts*
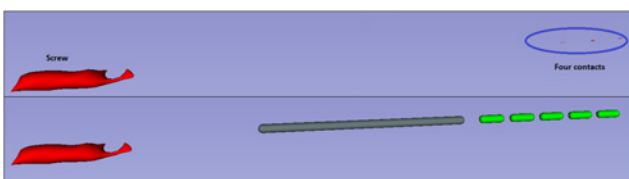

Fig. 6 *False electrode identification problem: result of the step-3 for a 15-contact electrode (top) and reconstructed 5-contact electrode at step-4 (bottom)*

type even with missing information using electrode's length specifications.

The output of the four previous steps is a visualisation in two-dimensional (2D) and 3D of the detected electrodes and contacts. A file with information related to the number of electrodes, the number of contacts in each electrode and the location of the different contact centres is also provided.

3. Results: We have tested the proposed automatic algorithm on the CT post-operative images of four patients. The respective numbers of electrodes and electrodes models are summarised in Table 1. The automatic segmentation has been run once, and the interactive segmentation has been performed by one user. The results are presented below. For patient case #1, an additional user has also performed the interactive segmentation.

Fig. 7 shows visual results of the interactive segmentation by one of the participants using the *one-by-one* method on patient case # 1: the 177 contacts of the 14 electrodes interactively clicked by the user are displayed in blue.

An example of the results of the fast interactive method is illustrated for the same patient in Fig. 8. Straight orange cylinders have been created between entry and target points.

We show in Fig. 9 the electrodes and contacts obtained from the same image using the automatic segmentation. The screws are presented in grey and the contacts in green.

In Fig. 10, the contacts obtained for case #1 using the interactive *one-by-one* method and the automatic segmentations are superimposed for visual comparison. Both methods provide small cylinders so that their respective positions can easily be compared. We can already observe that in most cases the depth of the contacts along the electrodes has been well estimated by the automatic algorithm. However, a major difference is that the interactive method produces

Table 1 Distribution of electrodes (from DIXI Medical) for the four patients

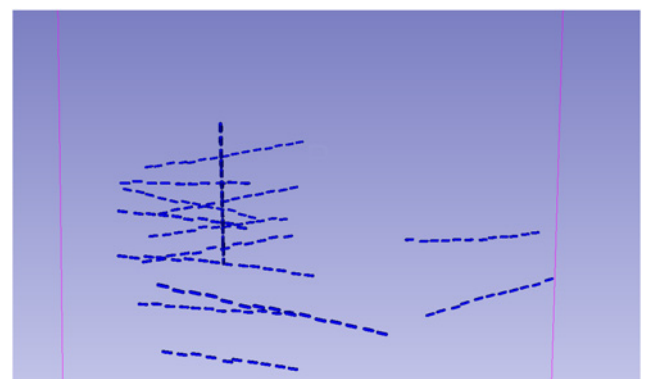|	Number of electrodes	Type of electrodes
case #1	14	15AM (5×), 12AM (6×), 10AM (3×)
case #2	18	15AM (6×), 15CM (1×), 12AM (5×), 10AM (4×), 8AM (2×)
case #3	15	18AM (1×), 15AM (5×), 12AM (4×), 10AM (3×), 8AM (2×)
case #4	15	18AM (3×), 12AM (6×), 10AM (5×), 8AM (1×)

Fig. 7 *Segmented electrodes using the one-by-one interactive method. Contacts are represented in blue*
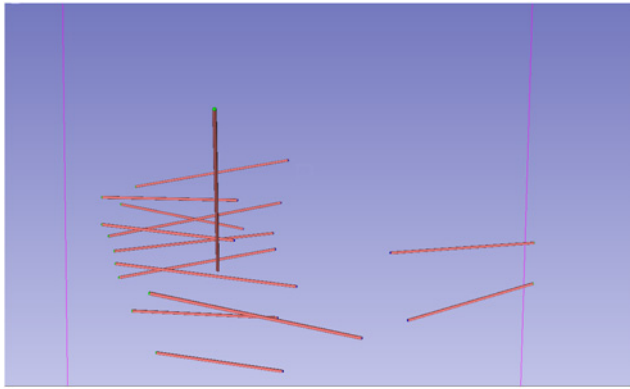
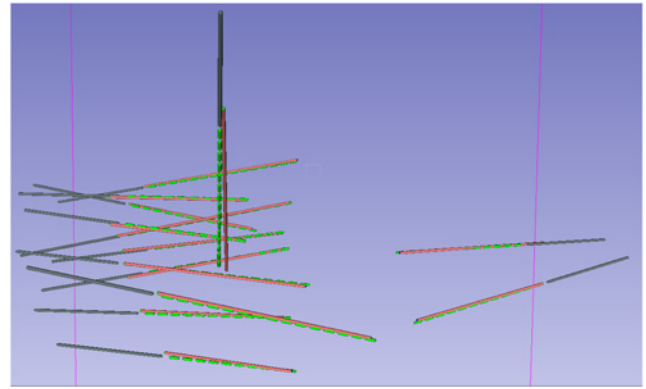**Fig. 8** *Segmented electrodes using the fast interactive method. Orange cylinders represent the electrodes*
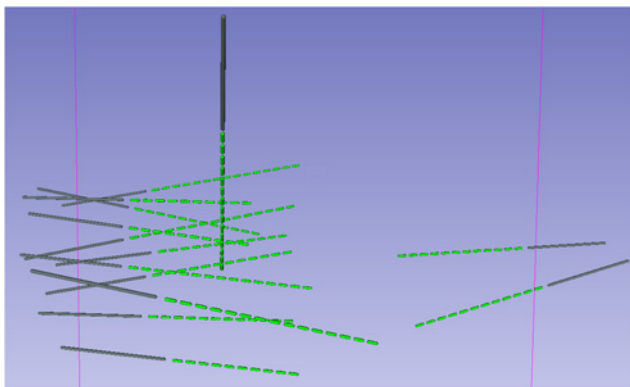

Fig. 9 *Segmented electrodes using the automatic detection algorithms. Contacts are in green and screws are in grey*
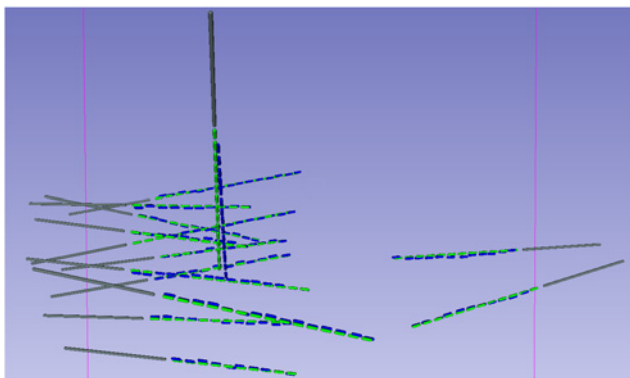

Fig. 10 *Superposition of the contacts obtained by one-by-one interactive and automatic methods*

shapes of irregular curvature, whereas the automatic method produces smooth straight shapes.

When superimposing the results of the second interactive (*fast*) method (Fig. 11), we can visually compare the main directions of the electrodes shapes. We can observe that most of them are relatively close to the interactive results.

3.1. Accuracy

3.1.1 *Accuracy of the contacts centres position:* To compare the interactive and automatic approaches in terms of accuracy, we have calculated for each electrode the mean of Euclidean distances

Fig. 11 *Superposition of the contacts obtained by fast interactive and automatic methods*

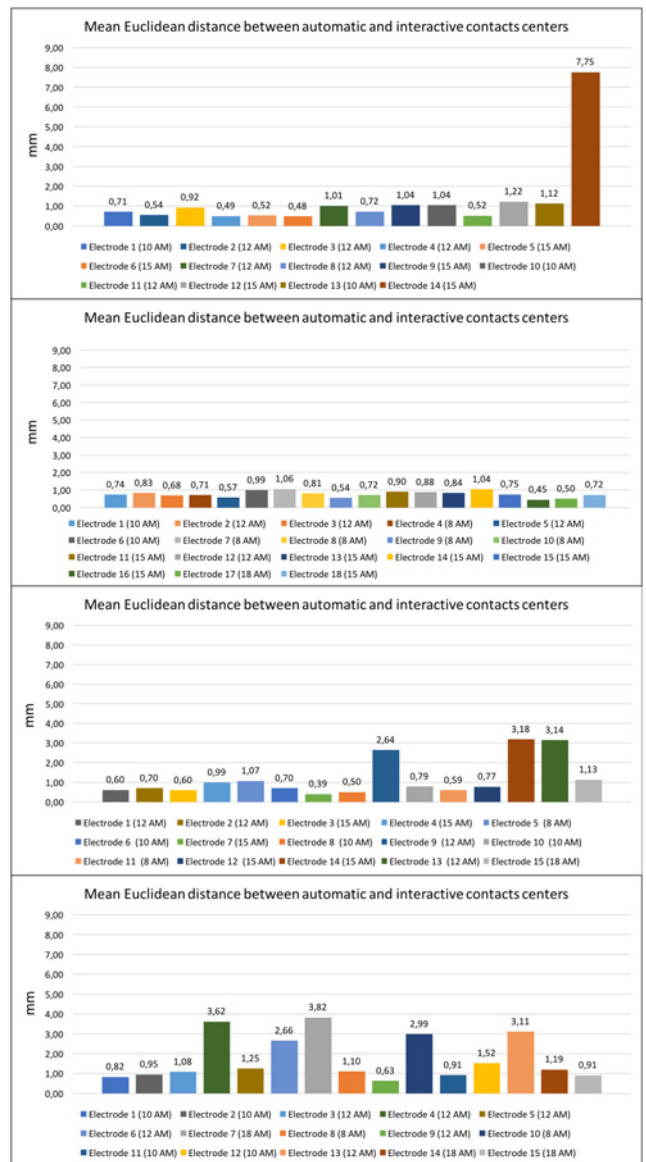**Fig. 12** *Contacts location comparison for patients cases # 1, 2, 3, 4 (from top to bottom): mean of Euclidean distances between automatic and interactive centres. Values are given in millimetres*

between each electrode contact centre obtained interactively by the *one-by-one* method and the corresponding contact calculated automatically. For the four cases, the comparisons have been performed
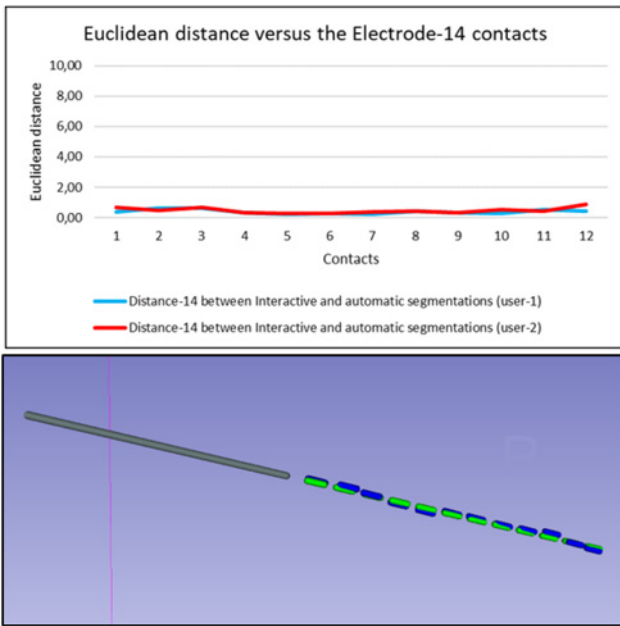
Fig. 13 *Result with the lowest difference between automatic (green) and interactive (blue) contacts location (Electrode-11). Blue curve: user-1 results, red curve: user-2 results. Values are given in millimetres*
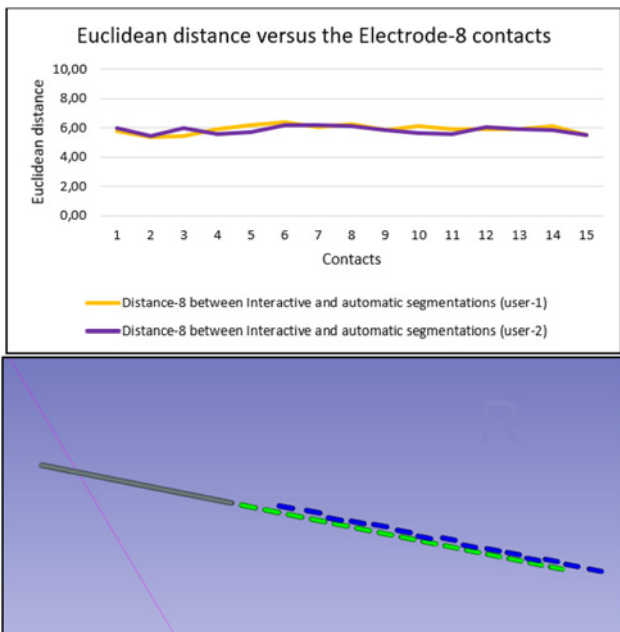

Fig. 14 *Result with the highest difference between automatic (green) and interactive (blue) contacts location (Electrode-14). Yellow curve: user-1 results and purple curve: user-2 results. Values are given in millimetres*

only with user-1 who tested on all cases. Results obtained for the four patients are displayed on the charts of Fig. 12.

When comparing the results obtained by the two users on the same patient case (#1), we can observe that in both cases the best results (with the lowest difference between locations of interactive and automatic centres) are obtained for Electrode-11. Fig. 13 gives the distribution of Euclidean distances between the centres in function of the associated contact number and a zoom in on Electrode-11 segmentations (interactive in blue and automatic in green/grey). On the two curves in Fig. 13, we can observe that the distance separating centres of contacts segmented automatically

Table 2 Electrodes axes comparison: max, min and average angles between the automatic direction and the *fast* interactive direction

	Max angle	Min angle	Average angle
case #1	3.30	0.34	1.35
case #2	1.89	0.11	0.93
case #3	3.38	0.23	1.41
case #4	13.2	0.12	2.69

Angles are given in degrees.

Table 3 Execution times for the automatic and interactive segmentations for the four patients

	Case #1	Case #2	Case #3	Case #4
one-by-one	8′ 51″	11′ 20″	10′ 10″	13′ 10″
fast interactive	3′ 27″	5′ 10″	4′ 24″	5′ 22″
automatic	2′ 6″	2′ 39″	1′ 41″	1′ 25″

and interactively stays very close to 0 for all of the 12 contacts (respective averages of 0.39 and 0.48 mm for the two participants).

On the contrary, the most imprecise result while comparing interactive and automatic contact centres location is obtained for both users in the case of Electrode-14 that contains 15 contacts and for which the variation of the distance between contacts is shown in Fig. 14 as well as the electrode segmentation. For this electrode, the average distance is 5.92 and 5.85 mm. We can note that the distance seems to be mainly a problem with the depth of the contacts.

A two sample *t*-test shows that there is no significant difference in the results between the two participants (*p*-value>0.05).

As for comparing the automatic and the interactive centres locations, we can observe in Fig. 12 that the average distance stays lower than 2 mm for the majority of electrodes (Patient 1: 87% of electrodes, Patient 2: 100%, Patient 3: 80% and Patient 4: 67%. However, some electrodes are still presenting a large difference concerning contacts location. Those electrodes seem to be having missing contacts (compare Fig. 6).

3.1.2 Accuracy of the electrodes axes direction: Another important element to consider while assessing the automatic algorithm accuracy is the electrodes axes direction. Consequently, axes directions obtained using the fast interactive method have been compared with the axes directions returned by the automatic algorithm by measuring the angle between them. The maximum, minimum and average angles are computed for each of the four cases and are summarised in Table 2; *N.B.* Given a patient, the average angle corresponds to the average of the angles obtained for all the electrodes inserted in that patient's brain.

3.2. Execution time: Table 3 summarises the execution times on the four patients' images for the automatic algorithm and the interactive approach by user-1. For the automatic method, the preprocessing time is included. The obtained results show that the proposed automatic segmentation is significantly faster than both of the interactive segmentations.

4. Discussion and conclusion: In the previous sections, we have presented two interactive and an automatic approach to segment SEEG electrodes in the post-operative phase. The results that we have obtained on a few patient cases show that the proposed automatic algorithm was able to segment a large majority of electrodes with a reasonable accuracy compared with the *one-by-one* interactive method. A few exceptions remain, for

which the accuracy could be improved, mostly due to a small number of undetected contacts. The automatic method showed a good approximation of the real position of electrodes contacts and seems to be a promising method. The automatic algorithm does not require any intervention from the user and performs automatically all the SEEG electrodes detection procedure including the preprocessing phase.

Compared to the literature, after the preprocessing phase, the automatic algorithm we proposed has the advantage to perform a completely automatic segmentation of the SEEG electrodes without the need of any preoperative information or surgeon inter-action, unlike the method proposed in [3]. The method proposed by the authors is based on data coming from the preoperative planning phase to obtain entry and target points for each electrode, calculates its axis and then determines its contacts positions. In our case, we propose an automatic classification of contacts that are directly carried out from the PCA calculated axes from screws without any prior information, and then automatically adjust the contacts locations depending on the geometrical characteristics of the electrodes.

A future improvement of the automatic algorithm is to take into account electrodes bending, by shifting the automatically segmented contacts so that they could respect the electrodes curvature and further minimise the error. Indeed, the segmentation results obtained after step-3 already allows to have contacts that respect the actual curvature of the electrodes. It would be feasible to use this information to produce curved electrode shapes. The method proposed very recently by Granados *et al.* [4] is probably the most interesting and closest to our works. They take into account electrode bending and require a few if not none interaction. The detected contacts are visualised as points. Our method is also able to detect the electrode model and allows to visualise the detected contacts using the actual shape and spacing of the electrode.

Concerning the execution times, Table 3 shows that the automatic algorithm is fast and competitive with the *fast* interactive method. It is a great benefit for the surgeon, who will be freed from a tedious task, and spare time that can be dedicated to another task. Furthermore, we could imagine that such an automatic method could allow for a systematic extraction of contacts localisations on massive retrospective datasets, in order to feed a deep learning algorithm in the context of the preoperative planning of SEEG implantation. Current approaches for preoperative planning of electrodes trajectories [7–9] use conventional methods, and it could be interesting to compare them with machine learning methods if the number of examples is sufficient, which would require a huge work of post-operative contacts detection.

Regarding the accuracy, the principal axes of the automatically segmented electrodes are almost superimposed for the majority of electrodes as shown in Table 2. This promising result further confirms that the automatic method seems to approximate the reality quite well. However, further investigations and tests are still needed to find out a generalised solution to the aforementioned remaining challenges.

6 References

[1] Talairach J., Bancaud J.: 'Stereotaxic approach to epilepsy', in Krayenbühl H., Maspes P.E., Sweet W.H. (Eds.): 'Progress in neurological surgery', vol. 5 (Karger Publishers, Basel, 1973), pp. 297–354

[2] Guénot M., Isnard J., Ryvlin P., ET AL.: 'SEEG-guided RF thermocoagulation of epileptic foci: feasibility, safety, and preliminary results', *Epilepsia*, 2004, **45**, (11), pp. 1368–1374

[3] Arnulfo G., Narizzano M., Cardinale F., ET AL.: 'Automatic segmentation of deep intracerebral electrodes in computed tomography scans', *BMC Bioinf.*, 2015, **16**, (1), p. 99

[4] Granados A., Vakharia V., Rodionov R., ET AL.: 'Automatic segmentation of stereoelectroencephalography (SEEG) electrodes post-implantation considering bending', *Int. J. Comput. Assist. Radiol. Surg.*, 2018, **13**, (6), pp. 935–946

[5] D'Albis T., Haegelen C., Essert C., ET AL.: 'PyDBS: an automated image processing workflow for deep brain stimulation surgery', *Int. J. Comput. Assist. Radiol. Surg.*, 2015, **10**, (2), pp. 117–128

[6] Fedorov A., Beichel R., Kalpathy-Cramer J., ET AL.: '3D slicer as an image computing platform for the quantitative imaging network', *Magn. Reson. Imaging*, 2012, **30**, (9), pp. 1323–1341

[7] De-Momi E., Caborni C., Cardinale F., ET AL.: 'Multi-trajectories automatic planner for stereoelectroencephalography (SEEG)', *Int. J. Comput. Assist. Radiol. Surg.*, 2014, **9**, (6), pp. 1087–1097

[8] Sparks R., Zombori G., Rodionov R., ET AL.: 'Automated multiple trajectory planning algorithm for the placement of stereoelectroencephalography (SEEG) electrodes in epilepsy treatment', *Int. J. Comput. Assist. Radiol. Surg.*, 2017, **12**, (1), pp. 123–136

[9] Sparks R., Vakharia V., Rodionov R., ET AL.: 'Anatomy-driven multiple trajectory planning (ADMTP) of intracranial electrodes for epilepsy surgery', *Int. J. Comput. Assist. Radiol. Surg.*, 2017, **12**, (8), pp. 1245–1255